Clim. Past Discuss., doi:10.5194/cp-2016-105, 2016
Manuscript under review for journal Clim. Past
Published: 31 October 2016

Climate of the Past Discussions

Holocene dynamics in the Bering Strait inflow to the Arctic and the Beaufort Gyre circulation based on sedimentary records from the Chukchi Sea

Masanobu Yamamoto[1,2*], Seung Il Nam[3], Leonid Polyak[4], Daisuke Kobayashi[2], Kenta Suzuki[2], Tomohisa Irino[1,2], Koji Shimada[5]

[1]Faculty of Environmental Earth Science, Hokkaido University, Kita-10, Nishi-5, Kita-ku, Sapporo 060-0810 Japan

[2]Gradute School of Environmental Science, Hokkaido University, Kita-10, Nishi-5, Kita-ku, Sapporo 060-0810 Japan

[3]Korea Polar Research Institute, 26 Songdomirae-ro, Yeonsu-gu, Incheon 21990, Republic of Korea

[4]Byrd Polar and Climate Research Center, The Ohio State University, , Columbus, OH 43210USA

[5]Tokyo University of Marine Science and Technology, 4-5-7, Konan, Minato-ku, Tokyo 108-8477, Japan.

**Corresponding author. Tel: +81-11-706-2379, Fax: +81-11-706-4867, E-mail address: myama@ees.hokudai.ac.jp (M. Yamamoto)*

ABSTRACT

The Beaufort Gyre (BG) and the Bering Strait inflow (BSI) are important elements of the Arctic Ocean circulation system and major controls on the distribution of Arctic sea ice. We report records of the quartz/feldspar and chlorite/illite ratios in two sediment cores from the northern Chukchi Sea providing insights into the long-term dynamics of

Clim. Past Discuss., doi:10.5194/cp-2016-105, 2016
Manuscript under review for journal Clim. Past
Published: 31 October 2016

Climate of the Past
Discussions

the BG circulation and the BSI during the Holocene. The quartz/feldspar ratio, a proxy of the BG strength, gradually decreased during the Holocene, suggesting a long-term decline in the BG strength, consistent with orbitally-controlled decrease in summer insolation. We suppose that the BG rotation weakened as a result of increasing stability of sea-ice cover at the margins of the Canada Basin, driven by decreasing insolation. Millennial to multi-centennial variability in the quartz/feldspar ratio (the BG circulation) is consistent with fluctuations in solar irradiance, suggesting that solar activity affected the BG strength on these timescales. The BSI, approximated by the chlorite/illite record, shows intensified flow from the Bering Sea to the Arctic during the middle Holocene, which is attributed primarily to the effect of an overall weaker Aleutian Low. This middle Holocene strengthening of the BSI was coeval with intense subpolar gyre circulation in the North Atlantic. We propose that the BSI is linked with the North Atlantic circulation via an atmospheric teleconnection between the Aleutian and Icelandic Lows. A correspondence between the Holocene variability of the BSI and North Atlantic Drift suggests that this connection is involved in a mechanism muting salinity changes in the North Atlantic, and thereby stabilizing the Atlantic Meridional Overturning Circulation.

1. Introduction

The Arctic currently faces rapid climate change caused by global warming (e.g., Screen and Simmonds, 2010; Harada, 2016). Changes in the current system of the Arctic Ocean regulate the state of Arctic sea ice and are involved in global processes via ice albedo feedback and the delivery of freshwater to the North Atlantic Ocean (Miller et al., 2010; Screen and Simmonds, 2010). The most significant consequence of this climate change during recent decades is the retreat of summer sea ice in the Pacific sector of the Arctic (e.g., Harada et al., 2016, and references therein). Inflow of warm Pacific water through the Being Strait (hereafter Bering Strait Inflow [BSI]) is suggested to have caused catastrophic changes in sea ice stability in the western Arctic Ocean (Shimada et al., 2006). Comprehending these changes requires investigation of a longer-term history of circulation in the western Arctic and its relationship to atmospheric forcings. Within this context, the Chukchi Sea is a key region to understand the western Arctic current system as it is located at the crossroads of the BSI and the Beaufort Gyre (BG) circulation in the western Arctic Ocean (Fig. 1) (e.g., Winsor and Chapman, 2004; Weingartner et al., 2005).

In this paper we apply mineralogical proxies of the BG and BSI to sediment cores with a century-scale resolution from the northern margin of the Chukchi shelf. The generated record provides new understanding of changes in the BG circulation and BSI strength during most of the Holocene (last ~9 ka). We discuss the possible causes and forcings of the BG and BSI variability, as well as its relationship to sea-ice history in the western Arctic and the linkage with North Atlantic Ocean dynamics.

2. Background information

2.1. Oceanographic settings

The wind-driven surface current system of the Arctic Ocean consists of the BG and the Transpolar Drift (TPD) (Proshutinsky and Johnson, 1997; Rigor et al., 2002). This circulation is controlled by the atmospheric system known as the Arctic Oscillation (AO) (Rigor et al., 2002). When the AO is in the positive phase, the BG shrinks back into the Beaufort Sea, the TPD expands to the western Arctic Ocean, and the sea-ice

Clim. Past Discuss., doi:10.5194/cp-2016-105, 2016
Manuscript under review for journal Clim. Past
Published: 31 October 2016

transport from the eastern Arctic to the Atlantic Ocean is intensified. When the AO is in negative phase, the BG expands, the TPD is limited to the eastern Arctic, and sea ice is exported efficiently from the Canada Basin to the eastern Arctic. Thus, sea-ice distribution is closely related to the current system.

A dramatic strengthening of the BG circulation occurred during the last two decades (Shimada et al., 2006; Giles et al., 2012). This change was attributed to a recent reduction in sea-ice cover along the margin of the Canada Basin, which caused a more efficient transfer of the wind momentum to the ice and underlying waters in the BG (Shimada et al., 2006). The delayed development of sea ice in winter enhanced the western branch of the Pacific Summer Water across the Chukchi Sea. This anomalous heat flux into the western part of the Canada Basin retarded sea-ice formation during winter, thus, further accelerating overall sea-ice reduction.

The BSI, an important carrier of heat and freshwater to the Arctic, transports the Pacific water to and across the Chukchi Sea, interact with the BG circulation at the Chukchi shelf margin (e.g., Shimada et al., 2006). After passing the Bering Strait the BSI flows in three major branches. One branch, the Alaskan Coastal Current (ACC), runs northeastward along the Alaskan coast as a buoyancy-driven boundary current (Red arrow in Fig. 1; Shimada et al., 2001; Pickart, 2004; Weingartner et al., 2005). The second, central branch follows a seafloor depression between Herald and Hanna Shoals, then turns eastward and merges with the ACC (Yellow arrow in Fig. 1; Winsor and Chapman, 2004; Weingartner et al., 2005). The third branch flows northwestward, especially when easterly winds prevent the ACC (Winsor and Chapman, 2004). This branch may then turn eastward along the shelf break (Blue arrow in Fig. 1; Pickart et al., 2010).

Clim. Past Discuss., doi:10.5194/cp-2016-105, 2016
Manuscript under review for journal Clim. Past
Published: 31 October 2016

Climate of the Past Discussions

The BSI is driven by a northward dip in sea level between the North Pacific and the Arctic Ocean (Shtokman, 1957; Coachman and Aagaard, 1996). There has been a long-standing debate, whether this dipping is primarily controlled by steric difference (Stigebrandt, 1984) or from wind-driven circulations (Gudkovitch, 1962). Stigebrandt (1984) assumed that the salinity difference between the Pacific and Atlantic Oceans causes the steric height difference between the Bering Sea and the Arctic Ocean. Aagaard et al. (2006) argued that the local salinity in the northern Bering Sea controlled the BSI, although wind can considerably modify the BSI on a seasonal timescale. De Boer and Nof (2004) proposed a model that the mean sea level difference along the strait is set up by the global winds, particularly the strong Subantarctic Westerlies.

Recently, a conceptual model of the BSI controls has been developed based on a decade of oceanographic observations (Danielson et al., 2014). According to this model, storms centered over the Bering Sea excite continental shelf waves on the eastern Bering shelf that intensify the BSI on synoptic time scales, but the integrated effect of these storms tends to decrease the BSI on annual to decadal time scales. At the same time, an eastward shift and overall strengthening of the Aleutian Low pressure center during the period between 2000–2005 and 2005–2011 increased the sea level pressure in the Aleutian Basin south of the Bering Strait by 5 hPa, thus decreasing the water column density through isopycnal uplift by weaker Ekman suction. This change thereby raised the dynamic sea surface height by 4.2 m along the Bering Strait pressure gradient, resulting in the BSI increase by 4.5 cm/s, or 0.2 Sv (calculated based on the cross-section area of 4.25×10^6 m^2). This increase constitutes about one quarter of the average long-term BSI volume of ~0.8 Sv (Roach et al., 1995). Such a large contribution clearly identifies changes in the Aleutian Low strength and position as a key factor regulating the BSI on inter-annual time scales.

The BSI transfers not only heat but also freshwater. Pacific water contributes one-third of the total freshwater input to the Arctic Ocean (Woodgate and Aagaard, 2005). Modeling studies have suggested that the increased flow of fresh Pacific water through the Bering Strait can reduce the Atlantic meridional overturning circulation (AMOC) (Shaffer and Bendtsen, 1994; Hasumi, 2002; Hu et al., 2005). Subsequent studies proposed mechanisms stabilizing the AMOC, when the Bering Strait is open (e.g., De Boer and Nof, 2004; Keigwin and Cook, 2007). De Boer and Nof (2004) assumed that the discharged freshwater in the North Atlantic can be flushed out through the Bering Strait to the Pacific, thus stabilizing the AMOC. Keigwin and Cook (2007) suggested a negative feedback mechanism involving warm anomalies in the North Atlantic. Such anomalies supposedly drive fresher BSI via increasing moisture transport from the tropical Atlantic to Pacific and stronger East Asian summer monsoon, accordingly suppressing the Atlantic meridional overturning and reducing the heat flux from the low to high-latitude North Atlantic. These perspectives are important for considering the difference in the stability of climate and the AMOC between the last glacial period and the Holocene (Dansgaard et al., 1993; Böhm et al., 2014). The open Bering Strait during interglacials could explain a more stable climate compared to glacial times, when the Bering Strait was closed to throughflow due to low sea level. The role of the BSI in these changes has, however, not been sufficiently investigated.

2.2. Mineral distribution in the Chukchi Sea sediments

Spatial variation in mineral composition of surficial sediments along the western Arctic margin has been investigated in a number of studies using different methodological approaches but showing an overall consistent picture (e.g., Naidu et al., 1982; Naidu and Mowatt, 1983; Kalinenko, 2001; Darby et al., 2011; Kobayashi et al., 2016). A recent study of mineral distribution in sediments from the Chukchi Sea and adjacent areas of the Arctic Ocean and the Bering Sea suggests that the quartz/feldspar (Q/F) ratio is higher on the North American than on the Siberian side of the western Arctic (Fig. 2; Kobayashi et al., 2016). These results are consistent with earlier studies including mineral determinations of shelf sediments and adjacent coasts (Vogt, 1997; Stein, 2008; Darby et al., 2011). In particular, data of Darby et al. (2011), although quantified by a different method, also show a trend of decreasing Q/F ratio from North American margin to the Chukchi Sea and further to the East Siberian Sea. This zonal gradient of the Q/F ratio suggests that quartz-rich but feldspar–depleted sediments are derived from the North American margin by the BG circulation, whereas feldspar–rich sediments are delivered to the Chukchi Sea from the Siberian margin by currents along the East Siberian slope. Thus, this ratio can be used as a provenance index for the BG circulation reflecting changes in its intensity in sediment-core records.

Kobayashi et al. (2016) also indicate that both the (chlorite + kaolinite)/illite and chlorite/illite ratios (CK/I and C/I ratios, respectively) are higher in the Bering Sea and decrease northward throughout the Chukchi Sea, reflecting the diminishing strength of the BSI (Fig. 2). These results are consistent with earlier studies showing that illite is a common clay mineral in Arctic sediments (Kalinenko, 2001; Darby et al., 2011), whereas, chlorite is more abundant in the Bering Sea and the Chukchi shelf areas influenced by the BSI (Naidu and Mowatt, 1983; Kalinenko, 2001; Nwaodua et al., 2014; Kobayashi et al., 2016). Chlorite occurs abundantly near the Bering Sea coasts of Alaska, Canada, and the Aleutian Islands (Griffin and Goldberg, 1963). The chlorite/illite ratio is higher in the bed load of rivers and deltaic sediments from southwestern Alaska than from northern Alaska and East Siberia, reflecting differences in the geology of the drainage basins (Naidu and Mowatt, 1983). Because chlorite grains are more mobile than illite grains under conditions of intense hydrodynamic activity, chlorite grains are transported a long distance from the northern Bering Sea to the Chukchi Sea via the Bering Strait (Kalinenko, 2001). In the surface sediments of the Chukchi Sea, the CK/I ratio shows a good correlation with the C/I ratio, indicating that both ratios can be used as a provenance index for the BSI (Kobayashi et al., 2016).

Ortiz et al. (2009) constructed the first chlorite-based Holocene record of the BSI by quantifying the total chlorite plus muscovite abundance based on diffuse spectral reflectance of sediments from a northeastern Chukchi Sea core. The record shows a prominent intensification of the BSI in the middle Holocene. However, a record from just one site is clearly insufficient to characterize sedimentation and circulation history in such a complex area. More records of mineral proxy distribution covering various oceanographic and depositional environments are needed to further our understanding of the evolution of the BSI.

The Holocene dynamics of the BG circulation is also poorly understood. A study of sediment core from the northeastern Chukchi slope identified centennial- to millennial-scale variability in the occurrence of Siberian iron oxide grains presumably delivered via the BG (Darby et al., 2012). However, transport of these grains depends not only on the BG, but also on circulation and ice conditions in the Eurasian basin, which complicates the interpretation and necessitates further proxy studies of the BG history.

3. Samples and methods

This study uses two sediment cores from the northeastern margin of the Chukchi Sea: ARA02B 01A-GC (gravity core) and HLY0501-05JPC/TC (jumbo piston core/trigger) collected from 111 m and 462 m water depth, respectively (Fig. 1). The sediments in 01A-GC and in the Holocene part of 05JPC consist predominantly of clayey silt. Age was constrained by seven accelerator mass spectrometry (AMS) ^{14}C ages of mollusc shells from core 01A-GC (Table 1) and six AMS ^{14}C ages from core 05JPC (Barletta et al., 2008; Darby et al., 2009). Concurrent age constraints for 05JPC were provided by ^{210}Pb determinations in the upper part (05TC) and paleomagnetic analysis (Barletta et al., 2008; McKay et al., 2008; Darby et al., 2012). ^{14}C ages were converted to calendar ages using the CALIB7.0 program and marine13 dataset (Reimer et al., 2013). Local reservoir corrections (ΔR) were assumed 500 years for 01A-GC and 0 years for 05JPC based on different water masses at the core sites (McNeely et al., 2006; Darby et al., 2012).

In total 110 samples were collected for mineralogical analysis from core 01A-GC at intervals averaging 5 cm (equivalent to approximately 80–90 years) down to a depth of 545 cm (ca. 9.3 ka), and 44 samples were collected from core 05JPC at intervals averaging 30 cm (equivalent to approximately 210–220 years) down to a depth of 1310 cm (ca. 9.5 ka).

We also analyzed 16 surface sediment samples (0–1 cm) from the eastern Beaufort Sea near Mackenzie delta and 3 surface sediment samples (0–1 cm) from the western

Beaufort Sea (Fig. 1) to fill the gaps in the dataset of Kobayashi et al. (2016). These were obtained during the RV Araon cruises in 2013 and 2014 (ARA04C and ARA05C, respectively; supplementary table 1).

Bulk mineral composition was analyzed on MX-Labo X-ray diffractometer (XRD) equipped with a CuKα tube and monochromator. The used tube voltage and current were 40 kV and 20 mA, respectively. Scanning speed was 4°2θ/min and the data sampling step was 0.02°2θ. Each powdered sample was mounted on a glass holder with a random orientation and X-rayed from 2 to 40°2θ. In this study, the background-corrected diagnostic peak intensity was used for evaluating the abundance of each mineral. The relative XRD intensities of quartz at 26.6°2θ (d = 3.4 Å), and feldspar including both plagioclase and K-feldspar at 27.7°2θ (d = 3.2 Å) were determined using MacDiff software (Petschick, 2000) based on the peak identification protocols of Biscaye (1965). The standard error of duplicate analyses in all samples averaged 1.1 for Q/F ratio.

Clay minerals (less than 2-μm diameter) in core 01A-GC were separated by the settling method based on the Stokes' law (Müller, 1967). To produce an oriented powder X-ray diffractometry (XRD) sample, the collected clay suspensions were vacuum-filtered onto 0.45-μm nitrocellulose filters and dried. Ethylene glycol (50 μl) was then soaked onto the oriented clay on the filters. Glycolated sample filters were stored in an oven at 70°C for four hours and then immediately subjected to XRD analyses. Analysis of clay mineral composition was conducted using a MAC Science MX-Labo XRD equipped with a CuKα tube and monochromator. Each sample filter was placed directly on a glass slide and X-rayed with a tube voltage of 40 kV and current of 20 mA. Scanning speed was 0.5°2θ/min and the data-sampling step was 0.02°2θ from 2 to 15°2θ. An additional precise scan with a scanning speed of 0.2°2θ/min and sampling step of 0.01°2θ from 24 to 27°2θ was conducted to distinguish chlorite from kaolinite by evaluation of the peaks around 25.1°2θ (Elvelhøi and Rønningsland, 1978). In this study, the background-corrected diagnostic peak intensity was used for evaluation of the abundance of each mineral. The relative XRD intensities of illite including mica at 8.8°2θ (d = 10.1 Å), chlorite including kaolinite (called "chlorite+kaolinite" hereafter) at 12.4°2θ (d = 7.1 Å), and chlorite at 25.1°2θ (d = 3.54 Å) were determined using MacDiff software (Petschick, 2000). The standard errors of duplicate analyses in all samples averaged 0.05 and 0.06 for CK/I and C/I ratios, respectively. The diffraction intensity of chlorite+kaolinite at 7.1 Å was significantly positively correlated with that of chlorite at 3.54 Å (r = 0.89), but not with that of kaolinite at 3.59 Å in western Arctic surface sediments (r = 0.39; Kobayashi et al., 2016), indicating that the diffraction intensity of chlorite+kaolinite is governed by the amount of chlorite rather than that of kaolinite.

Spectral analysis of the downcore Q/F variability was performed using the maximum entropy method provided in the Analyseries software package (Paillard et al., 1996).

4. Results

4.1. Surface sediments of the Beaufort Sea

Because the dataset of Kobayashi et al. (2016) has only one sample in the eastern Beaufort Sea, we added the data of 16 samples from the eastern Beaufort Sea near Mackenzie delta and 3 samples from the western Beaufort Sea to fill the gaps in their dataset. The new combined dataset clearly shows that the surface sediments in the eastern Beaufort Sea have the higher Q/F and lower CK/I and C/I ratios (Fig. 2A–C; Supplementary table 1). The Q/F ratio showed a westward decreasing trend from the eastern Beaufort Sea to the East Siberian Sea and its offshore area (Fig. 2D). The CK/I and C/I ratios showed a northward decreasing trend in the Chukchi Sea and the Chukchi Borderland (Fig. 2E). These trends support the conclusion of Kobayashi et al. (2016) mentioning that the Q/F ratio can be used as a provenance index for the BG circulation reflecting a westward decrease in its intensity, and the CK/I and C/I ratios can be used as a provenance index for the BSI reflecting a northward decrease in its intensity. The provenance and transportation of these detrital minerals are discussed in detail in Naidu and Mowatt (1983), Kalinenko (2001), Nwaodua et al. (2014) and Kobayashi et al. (2016).

4.2. Cores 01A-GC and 05JPC/TC

Quartz, feldspar including plagioclase and K-feldspar, illite, chlorite and kaolinite were detected in the study samples. Plagioclase comprises a variety of anorthite to albite. Microscopic observations of smear slides for the study samples revealed that quartz and feldspar are the two major minerals in the composition of detrital grains.

The Q/F ratio in both cores 01A-GC and 05JPC/TC shows a gradual long-term decrease throughout the Holocene (Figs. 3A and 4A; Supplementary tables 2 and 3). In core 01A-GC studied in more detail, the Q/F ratio also indicates millennial- to century-scale variability with identifiable maxima at ca. 9.1, 8.1, 7.1, 6.0, 4.6, 2.2 and 0.9 ka, and minima at ca. 8.3, 7.6, 6.8, 5.0, 2.9, 1.7 and 0.3 ka (Fig. 3A). In core 05JPC/TC, the milllennial-scale variability is unclear because of lower age resolution provided by samples under study (Fig. 4A).

In core 01A-GC, both the CK/I and C/I ratios show a similar downcore pattern with millennial and multi-centennial variations (Fig. 3A; Supplementary table 2). The ratios show a general increase of the BSI after ca. 9.5 ka with the highest values occurring between 6 and 4 ka, and high ratios around 2.5 ka and 1 ka (Fig. 3A). In core 05JPC/TC higher ratios also occur in the middle Holocene, but no significant long-term trend can be recognized, presumably because of relatively low age resolution (Fig. 4B; Supplementary table 3).

5. Discussion

5.1. Holocene trend in the Beaufort Gyre circulation

A consistent decrease in the Q/F ratio in both cores under study (Fig. 5A) suggests that the BG weakened during the Holocene. This pattern is consistent with an orbitally-forced decrease in summer insolation at northern high latitudes from the early Holocene to present. High summer insolation likely melted sea ice in the Canada Basin, in particular in the coastal areas (Fig. 6). The evidence of lower ice concentrations at the Canada Basin margins in the early Holocene was shown in the fossil records of bowhead whale bones from the Beaufort Sea coast (Dyke and Savelle, 2001) and driftwood from northern Greenland (Funder et al., 2011). This condition could decrease the stability of the ice cover at the margins of the Canada Basin, which accelerated the rotation of the BG circulation (Fig. 6), by comparison with observations from recent decades (Shimada et al., 2006). A decrease in summer insolation during the Holocene should have increased the stability of sea-ice cover along the coasts, resulting in the weakening of the BG.

Recent observations show that the BG circulation is linked to the AO (Proshutinsky and Johnson, 1997; Rigor et al., 2002). In the negative phase of the AO, the Beaufort High strengthens and intensifies the BG. If the gradual weakening of the BG during the

Clim. Past Discuss., doi:10.5194/cp-2016-105, 2016
Manuscript under review for journal Clim. Past
Published: 31 October 2016

Holocene were attributed to atmospheric circulation only, a concurrent shift in the mean state of the AO from the negative to positive phase would be expected. This view, however, contradicts the existing reconstructions of the AO history showing multiple shifts between the positive and negative phase during the Holocene (e.g., Rimbu et al., 2003; Olsen et al., 2012). We, thus, infer that the decreasing Holocene trend of the BG circulation is attributed not to changes in the AO pattern, but rather to the increasing stability of the sea-ice cover in the Canada Basin.

Based on a Holocene sediment record off northeastern Chukchi margin, Darby et al. (2012) suggested strong positive AO-like conditions between 3 and 1.2 ka based on abundant ice-rafted iron oxide grains from the West Siberian shelf. In contrast, a mostly negative AO in the late Holocene can be inferred from mineralogical proxy data indicating a general decline of the BSI after 4 ka (Ortiz et al., 2009), which could be attributed to a stronger Aleutian Low (Danielson et al., 2014) that typically corresponds to the negative AO (Overland et al., 1999). Olsen et al. (2012) also concluded that the AO tended to be mostly negative from 4.2 to 2.0 ka based on a redox proxy record from a Greenland lake. In order to comprehend these patterns, we need to consider not only the atmospheric circulation, but also sea-ice conditions. Based on the Q/F record in this study, summer Arctic sea-ice cover shrank in the early to middle Holocene, so that fast ice containing West Siberian grains could less effectively reach the Canada Basin because sea ice would have melted on the way to the BG. Later in the Holocene the ice cover expanded, and West Siberian fast ice could survive and be incorporated into the BG. We infer, therefore, that sediment transportation in the BG is principally governed by the distribution of summer sea ice and the resultant stability of the ice cover in the Canada Basin.

5.2. Millennial variability in the BG circulation

In addition to the decreasing long-term trend, the Q/F ratio in 01A-GC clearly displays millennial- to century-scale variability (Fig. 5b). A comparison with the record of total solar irradiance (Steinhilber et al., 2009) shows a general correspondence, where stronger BG circulation (higher Q/F ratio) corresponds to higher solar irradiance (Fig. 5b). Variation in the Q/F ratio indicates a significant periodicity of 1000 years with weak periodicities of 530 and 350 year, consistent with prominent periodicities in the variation of total solar irradiance (Fig. 7) (Steinhilber et al., 2009). A ~300-year phase lag between the solar irradiance and the Q/F ratio may be attributed to the underestimation of local carbon reservoir effect. This pattern suggests that millennial-scale variability in the BG was principally forced by changes in solar irradiance. Because these changes are energetically much smaller than changes in the summer insolation caused by orbital forcing, we suppose that solar activity did not directly affect the stability of ice cover in the Canada Basin. Alternatively, we suggest that the solar activity signal was amplified by positive feedback mechanisms, possibly through changes in the stability of sea-ice cover and/or the atmospheric circulation in the northern high latitudes.

In addition to cycles consistent with the solar forcing, Darby et al. (2012) reported a 1,550 year cycle in the Siberian grain variation in the Chukchi Sea record. This cycle was, however, not detected in our data indicative of the BG variation (Fig. 7). This difference suggests that the occurrence of Siberian grains in the Chukchi Sea sediments primarily reflects the formation and transportation of fast ice in the eastern Arctic Ocean rather than changes in the BG circulation.

5.3. Holocene changes in the Bering Strait Inflow

5.3.1. Implications from mineral composition of the Holocene records

The higher CK/I and C/I ratios in core 01A-GC in the middle Holocene correspond to higher linear sedimentation rates estimated by interpolation between ^{14}C dating points (Fig. 3C). We assume that these higher sedimentation rates indicate intensified BSI, because fine sediment in the study area is mostly transported by currents from the Bering Sea and shallow southern Chukchi shelf (Kalinenko, 2001; Darby et al., 2009; Kobayashi et al., 2016).

Mineral composition derived from diffuse spectral reflectance in core HLY0501-06JPC (Fig. 1; Ortiz et al., 2009) indicates that chlorite + muscovite content is especially high in the middle Holocene between ca. 4 and 6 ka (Fig. 4D). This pattern is similar to the CK/I and C/I distributions in 01A-GC (Fig. 3B) suggesting that the BSI was overall intensified in the middle Holocene. On the other hand, core 01A-GC also shows high CK/I and C/I ratios at ~7, 2.5, and 1 ka (Fig. 3B), which are not reproduced in chlorite + muscovite content in core HLY0501-06JPC. This discrepancy between 01A-GC and 06JPC chlorite records may be related to either methodological differences (decomposition of Diffuse Spectral Reflectance vs. XRD measurements), variable sediment focusing at different water depths, or redistribution of the BSI water between different branches after passing the Bering Strait. Both the Alaskan Coastal Current (ACC) and the central current can transport sediment particles to the 06JPC area (red and yellow arrows, respectively, in Fig. 1; Winsor and Chapman, 2004; Weingartner et al., 2005). In comparison, the western branch is more likely to carry sediment particles to the site of 01A-GC (blue arrow in Fig. 1). More investigation is warranted on the difference in mineral composition between these records to test its relationship to circulation patterns, which may provide important insight into the history of BSI and its impact on the Chukchi Sea.

5.3.2. Causes of BSI variations

The timing of the initial postglacial flooding of the ~50-m-deep Bering Strait was estimated as between ca. 12 and 11 ka (Elias et al., 1992; Keigwin et al., 2006). Gradual intensification of the BSI inferred from the increase in chlorite content from ca. 9 to 6 ka may have been largely controlled by the widening and deepening of the Bering Strait with rising sea level, although other factors as discussed below yet need to be tested. After the sea level rose to nearly present position by ca. 6 ka, its influence on changes in the BSI volume was negligible.

The possible driving forces of the BSI at full interglacial sea level may include several controls. One is related to the sea surface height difference between the Pacific and Atlantic Oceans regulated by the atmospheric moisture transport from the Atlantic to the Pacific Ocean across Central America (Stigebrandt, 1984). Increase in this moisture transport during warm climatic intervals (Leduc et al., 2007; Richter and Xie, 2010; Singh et al., 2016) may have intensified the BSI. Salinity proxy data for the last 90 ka from the Equatorial East Pacific confirm increased precipitation during warm events, but also show the trans-Central America moisture transport may operate efficiently only during intervals with a northerly position of the Intertropical Convergence Zone due to orographic constraints (Leduc et al., 2007). The existing Holocene salinity records from the North Pacific (e.g., Sarnthein et al., 2004) do not yet provide sufficient material to test the impact of these changes on the BSI.

Interplay of the global wind field and the AMOC has been proposed as another potential control on the BSI (De Boer and Nof, 2004; Ortiz et al., 2012). Results of an analytical ocean modeling experiment (Sandal and Nof, 2008) based on the island rule (Godfrey, 1989) suggest that weaker Subantarctic Westerlies in the middle Holocene could decrease the near surface, cross-equatorial flow from the Southern Ocean to the North Atlantic, thus enhancing the BSI and Arctic outflow into the Atlantic. This hypothesis waits to be tested more thoroughly, including robust proxy records of the Subantarctic Westerlies over the Southern Ocean.

Finally, BSI can be controlled by the regional wind patterns in the Bering Sea (Danielson et al., 2014), as explained above in Section 2.1. Oceanographic observations of 2000-2011 clearly show a decadal response of the BSI to a change in the sea level pressure in the Aleutian Basin affecting the dynamic sea surface height along the Bering Strait pressure gradient. In order to conclude, if this relationship holds on longer time scales, longer-term records are needed from areas affected by the BSI and the Bering Sea pressure system.

A number of proxy records from the Bering Sea and adjacent regions, both marine and terrestrial, have been used to characterize paleoclimatic conditions related to changes in the Bering Sea pressure system (e.g., Barron et al., 2003; Anderson et al., 2005; Katsuki et al., 2009; Barron and Anderson, 2011; Osterberg et al., 2014). Various proxies used in these records consistently show that the Aleutian Low was overall weaker in the middle Holocene than in the late Holocene, opposite to the BSI strength inferred from our Chukchi Sea data. For example, multi-proxy data from the interior Alaska and adjacent territories (Kaufman et al., 2016, and references therein) indicate overall drier and warmer conditions in the middle Holocene, consistent with weaker

Aleutian Low and stronger BSI. Diatom records from southern Bering Sea indicate more abundant sea ice in the middle Holocene, also suggestive of a weaker Aleutian Low (Katsuki et al., 2009). Alkenone and diatom records from the California margin show that the sea surface temperature was lower in the middle Holocene, suggesting stronger northerly winds indicative of weaker Aleutian Low (Barron et al., 2003). Intensification of the Aleutian Low in the late Holocene, which follows from these results, would have decreased sea level pressure in the Aleutian Basin, and thus the strength of the BSI, consistent with overall lower BSI after ca. 4 ka inferred from the Chukchi Sea sediment-core data (Figs. 3-4). A considerable climate variability of the Bering Sea region captured in the upper Holocene records, some of which have very high temporal resolution, is also closely linked to the pressure system changes (Anderson et al., 2005; Porter, 2013; Osterberg et al., 2014; Steinman et al., 2014). In particular, weakening of the Aleutian Low is reflected in Alaskan ice (Porter, 2013; Osterberg et al., 2014) and lake cores (Anderson et al., 2005; Steinman et al., 2014) at intervals centered around ca. 2 and 1–0.5 ka BP, which may correspond to BSI increases in the Chukchi core 01A-GC at ca. 2.5 and 1 ka BP (Fig. 3), considering the uncertainties of the sparse age constraints in the upper Holocene and/or underestimation of reservoir ages. Overall, the Aleutian Low control on the BSI on century to millennial time scales is corroborated by ample proxy data in comparison with the other potential controls, although more evidence is still required for a comprehensive interpretation.

5.4. Ocean circulation and sea ice

Dinoflagellate cyst and biomarker IP_{25} records from several cores in the northeastern Chukchi Sea, including 05JPC, demonstrate that sea ice concentration in this area was overall higher in the early Holocene than in the middle and late Holocene (Figs. 8B and C; de Vernal et al., 2005; 2008; 2013; Farmer et al., 2011; Polyak et al., 2016). This pattern appears to contrast reconstructions from other Arctic regions that show lower sea-ice concentrations in the early Holocene (De Vernal et al., 2013). At the same time period, the summer sea ice probably retreated in the Beaufort Sea as indicated by regional whalebone distribution (Dyke and Savelle, 2001) and IP_{25} records from the straits of the Canadian Archipelago (Vare et al., 2009). This discrepancy suggests that the intensified BG circulation exported more ice from the Beaufort Sea to the northern Chukchi Sea margin. Furthermore, the heat transport from the North Pacific to the Arctic Ocean by the BSI was likely weaker in the early Holocene than at later times as indicated by mineralogical indicators of the North Pacific provenance (Figs. 3-4). We infer that this combination of stronger BG circulation and weaker BSI in the early Holocene resulted in increased sea-ice concentration in the Chukchi Sea despite high insolation levels (Fig. 6). In comparison, intense BSI, a crucial agent of heat transport from the North Pacific to the Arctic Ocean, along with weaker BG in the middle Holocene likely reduced sea ice cover in the Chukchi Sea. During the late Holocene, characterized by the weakest BG and moderate BSI, sea-ice conditions were intermediate and strongly variable (de Vernal et al., 2008, 2013; Polyak et al., 2016).

5.5. Linkage of the Bering Strait Inflow with the North Atlantic Ocean dynamics

Stronger BSI in the middle Holocene co-occurred with the strengthening of Irminger and Labrador Currents in the North Atlantic (Fig. 9; Thornalley et al., 2009). The sea surface temperature and salinity estimated from the Mg/Ca ratio and $\delta^{18}O$ of planktonic foraminifera were maximal in the middle Holocene at ODP Site 984 (Figs. 9B; Came et

Clim. Past Discuss., doi:10.5194/cp-2016-105, 2016
Manuscript under review for journal Clim. Past
Published: 31 October 2016

Climate of the Past
Discussions

al., 2007) and core RAPiD-12-1K (Fig. 9C; Thornalley et al., 2009) off Iceland, suggesting an intense Irminger Current. In cores AI07-3G and 12G near Newfoundland, the dinoflagellate cyst assemblages indicate a colder and fresher environment in the middle Holocene, which is consistent with a stronger Labrador Current (Fig. 9D; Solignac et al., 2011). For the same period, an intense East Greenland Current is indicated by higher $\delta^{13}C$ of planktic foraminifera in a Nordic Sea core (Bauch et al., 2001). The combination of these proxy records suggests an overall intensification of the subpolar gyre (SPG) circulation in the North Atlantic during the middle Holocene (Thornalley et al., 2009), coeval with the BSI strengthening implied by the Chukchi Sea proxy records.

The correspondence between the North Atlantic SPG circulation and climate variability in the northeast Pacific, such as the abrupt changes in Alaskan and Bering Sea climate at ~3–4 ka (e.g., Heusser et al., 1985; Barron et al., 2003; Katsuki et al., 2009), suggests atmospheric teleconnection in the northern high latitudes (Thompson and Wallace, 1998) as a key process linking the SPG and the BSI. This conclusion is consistent with the 20th century observations, indicating that the stronger/weaker Icelandic Low is associated with the weaker/stronger Aleutian Low in the positive/negative phase of the Arctic Oscillation (Thompson and Wallace, 1998; Overland et al., 1999; Honda et al., 2001; Sun and Tan, 2013). A 100-year long coralline alga record from the western Bering Sea indicates a statistically significant link between decadal fluctuations in sea level pressure in the North Pacific and North Atlantic (Hetzinger et al., 2012). The stronger Icelandic Low intensifies the SPG, and the weaker Aleutian Low simultaneously intensifies the BSI. Because seasonal distribution of sea ice and snow cover determines the atmospheric circulation patterns in

Clim. Past Discuss., doi:10.5194/cp-2016-105, 2016
Manuscript under review for journal Clim. Past
Published: 31 October 2016

the northern high latitudes, long-term changes in its spatial variability may have a major role in the Icelandic–Aleutian Low seesaw.

Despite the considerable changes in the SPG circulation in the North Atlantic during the Holocene (Thornalley et al., 2009), low-resolution proxy records indicate that ventilation in the Nordic Sea and North Atlantic was stable throughout the Holocene (Fig. 9D; McManus et al., 2004). A high-resolution record of carbon isotopes of benthic foraminifera indicates that the AMOC weakened temporarily at the time intervals of 6 to 5 ka and 3 to 2.5 ka (Fig. 3D; Oppo et al., 2003), which correspond to the inferred intensification of the BSI at 6 and 2.5 ka, respectively (Fig. 9A). This correspondence implies a possibility that the BSI controlled temporary weakening of the AMOC by the freshening of the North Atlantic water, as suggested by modeling studies (Shaffer and Benson et al., 1994; Hasumi, 2002). The recovery of the AMOC after these short-term weakening events suggests that some mechanism stabilized the AMOC during the Holocene.

Several hypotheses have been proposed to explain the stable AMOC in the Holocene. De Boer and Nof (2004) proposed that when the Bering Strait was closed, the AMOC stopped after the influx of freshwater into the North Atlantic, but the open Bering Strait provided flushing of freshwater from the North Atlantic to the Pacific via the Arctic Ocean, and thus the AMOC recovery. Keigwin and Cook (2007) hypothesized a negative feedback, where stronger AMOC induces freshening of the North Pacific surface water by a northward shift of the intertropical convergence zone and an intensified East Asian summer monsoon. These changes drive northward freshwater flow through the Bering Strait to the northern North Atlantic, thus suppressing the

AMOC. Evidence of a corresponding salinity change in the North Pacific is required to support this hypothesis.

Based on paleoceanographic proxy data from the Holocene records, we propose the following mechanism. In the middle Holocene, the stronger Icelandic Low drove the North Atlantic SPG circulation with a high influx of saline water from the lower latitudes (Fig. 10). At the same time, the weaker Aleutian Low enhanced the BSI, which increased freshwater flux from the North Pacific into the North Atlantic. In addition, the weaker Aleutian Low–stronger Icelandic Low pattern (positive phase of the Arctic Oscillation) would have increased precipitation in the Arctic Ocean (Serreze et al., 1995). This process would have also increased freshwater flux into the North Atlantic. The saline water from the tropical Atlantic was thus compensated by freshwater from the North Pacific and increased precipitation. Thornally et al. (2009) reported that the North Atlantic Current became more saline during enhanced Arctic freshwater flux to the subpolar North Atlantic in the middle Holocene, suggesting a negative feedback mechanism. Our data suggests that the Arctic freshwater flux was enhanced due to the intense influx of fresher Pacific water in the middle Holocene, combined with an inferred increase in Arctic precipitation. In the late Holocene, the weaker Icelandic Low and the stronger Aleutian Low caused lower fluxes of both the saline water and freshwater to the North Atlantic (Fig. 10). This mechanism muted salinity change and thereby stabilized the AMOC in the Holocene.

The compensational mechanism proposed above could not have fully operated during glacial periods because the Bering Strait was closed at low sea levels. This condition allowed much higher-amplitude fluctuations in the AMOC and climate than in the Holocene (e.g., Dansgaard et al., 1993; Böhm et al., 2014). Overall, our study identifies the linkage between the BSI and the AMOC as an important climate mechanism contributing to the relative stability of interglacial climates.

6. Conclusions

The sedimentary proxy-based reconstruction of the BG weakening during the Holocene, likely driven by the orbitally-controlled summer insolation decrease, indicates basin-wide changes in the Arctic current system and suggests that the stability of sea ice is a key factor regulating the Arctic Ocean circulation on the long-term (e.g., millennial) time scales. This conclusion helps to better understand a dramatic change in the BG circulation during the last decade, probably caused by sea-ice retreat along the margin of the Canada Basin and a more efficient transfer of the wind momentum to the ice and underlying waters (Shimada et al., 2006). These results suggest that the rotation of the BG is likely to be further accelerated by the projected future retreat of summer Arctic sea ice.

Our results on clay-mineral ratios quantifying inputs of chlorite from the Bering Sea to sediments at the northern Chukchi margin provide a robust record of the strength of the BSI during the Holocene. We conclude that BSI variability after the establishment of the full interglacial sea level was primarily controlled by the Bering Sea pressure system (strength and position of the Aleutian Low). Details of this mechanism, as well as contributions from other potential BSI controls, such as climatically-driven Atlantic-Pacific moisture transfer and the impact of global wind stress, need to be further investigated. Based on the generated record and its interpretation we propose a new concept that the BSI was linked with the North Atlantic subpolar gyre circulation via atmospheric teleconnection between the Icelandic and Aleutian lows, and their

Clim. Past Discuss., doi:10.5194/cp-2016-105, 2016
Manuscript under review for journal Clim. Past
Published: 31 October 2016

synchronized variations contributed to the stability of the AMOC and climate during the Holocene.

Acknowledgements

We thank all of the captain, crew and scientists of RV *Araon* for their help during the cruise of sampling. We also thank Yu-Hyeon Park, Anne de Vernal, Seth L. Danielson, Julie Brigham-Grette and Kaustubh Thirumalai for valuable discussion, So-Young Kim, Hyo-Sun Ji, Young-Ju Son, Duk-Ki Han and Hyoung-Jun Kim for assistance in coring and subsampling and Keiko Ohnishi for analytical assistance. The study was supported by a grant-in-aid for Scientific Research (B) the Japan Society for the Promotion of Science, No. 25287136 (to M.Y.) and Basic Research Project (PE16062) of Korean Polar Research Institute and the NRF of Korea Grant funded by the Korean Government (NRF-2015M1A5A1037243) (to S.I.N.).

References

Aagaard, K., Weingartner, T.J., Danielson, S. L., Woodgate, R.A., Johnson, G. C., and Whitledge, T.E.: Some controls on flow and salinity in Bering Strait, Geophysical Research Letters, 33, L19602, 2006.

Anderson, L, Abbott, M.B., Finney, B.P., and Burns, S.J.: Regional atmospheric circulation change in the North Pacific during the Holocene inferred from lacustrine carbonate oxygen isotopes, Yukon Territory, Canada, Quaternary Research, 64, 21–35, 2005.

Barletta, F. et al.: High resolution paleomagnetic secular variation and relative paleointensity records from the western Canadian Arctic: implication for Holocene

Clim. Past Discuss., doi:10.5194/cp-2016-105, 2016
Manuscript under review for journal Clim. Past
Published: 31 October 2016

stratigraphy and geomagnetic field behaviour, Canadian Journal of Earth Sciences, 45, 1265–1281, 2008.

Barron, J.A. and Anderson, L.: Enhanced Late Holocene ENSO/PDO expression along the margins of the eastern North Pacific, Quaternary International, 235, 3–12, 2011.

Barron, J.A., Heusser, L., Herbert, T., and Lyle, M.: High-resolution climatic evolution of coastal northern California during the past 16,000 years, Paleoceanography, 18, 1020, 2003.

Bauch, H.A., Erlenkeuser, H., Spielhagen, R.F., Struck, U., Matthiessen, J., Thide, J., and Heinemeier, J.: A mutiproxy reconstruction of the evolution of deep and surface waters in the subarctic Nordic seas over the last 30,000 yr, Quaternary Science Reviews, 20, 659–678, 2001.

Biscaye, P.: Mineralogy and sedimentation of recent deep-sea clay in the Atlantic Ocean and adjacent seas and oceans, Geological Society of America Bulletin, 76, 803–832, 1965.

Böhm, E., Lippold, J., Gutjahr, M., Frank, M., Blaser, P., Antz, B., Fohlmeister, J., Frank, N., Andersen, M.B., and Deininger, M.: Strong and deep Atlantic meridional overturning circulation during the last glacial cycle, Nature, 517, 73–76, 2014.

Calkin, P.E., Wiles, G.C., and Barclay, D.J.: Holocene coastal glaciation of Alaska, Quaternary Science Reviews, 20, 49–461, 2001.

Came, R.E., Oppo, D.W., and McManus, J.F.: Amplitude and timing of temperature and salinity variability in the subpolar North Atlantic over the past 10 k.y., Geology, 35, 315–318, 2007.

Coachman, L.K., and Aagaard, K.. On the water exchange through Bering Strait, Limnology and Oceanography, 11, 44–59, 1966.

Danielson, S.L., Weingartner, T.J., Hedstrom, K.S., Aargaard, K., Woodgate, R., Curchister, E., and Stabeno, P.J.: Coupled wind-forced controls of the Bering-Chukchi shelf circulation and the Bering Strait throughflow: Ekman transport, continental shelf waves, and variations of the Pacific-Arctic sea surface height gradient, Progress in Oceanography, 125, 40–61, 2014.

Dansgaard, W., Johnsen, S.J., Clausen, H.B., Dahl-Jensen, D., Gundestrup, N.S., Hammer, C.U., Hvidberg, C.S., Steffensen, J.P., Sveinbjörnsdottir, A.E., Jouzel, J., Bond, G.: Evidence for general instability of past climate from a 250-kyr ice-core record, Nature 364, 218 – 220, 1993.

Darby, D.A., Ortiz, J.D., Polyak, L., Lund, S., Jakobsson, M., and Woodgate, R.A.: The role of currents and sea ice in both slowly deposited central Arctic and rapidly deposited Chukchi-Alaskan margin sediments, Global and Planetary Change, 68, 58–72, 2009.

Darby, D.A., Myers, W.B., Jakobsson, M., and Rigor, I.: Modern dirty sea ice characteristic and sources: The role of anchor ice, Journal of Geophysical Research, 116, C09008, 2011.

Darby, D.A., Ortiz, J.D., Grosch, C.E., and Lund, S.P.: 1,500-year cycle in the Arctic Oscillation identified in Holocene Arctic sea-ice drift, Nature Geoscience, 5, 897–900, 2012.

De Boer, A.M. and Nof, D.: The exhaust valve of the North Atlantic, Journal of Climate, 17, 417–422, 2004.

de Vernal, A., Hillaire-Marcel, C., and Darby, D.A.: Variability of sea ice cover in the Chukchi Sea (western Arctic Ocean) during the Holocene, Paleoceanography, 20, PA4018, doi:10.1029/2005PA001157, 2005.

de Vernal A, Hillaire-Marcel C, Solignac S, et al.: Reconstructing sea ice conditions in the Arctic and sub-Arctic prior to human observations, Geophysical Monograph 180, American Geophysical Union, Washington, p. 27–45, 2008.

de Vernal, A. et al.: Dinocyst-based reconstructions of sea ice cover concentration during the Holocene in the Arctic Ocean, the northern North Atlantic Ocean and its adjacent seas, Quaternary Science Reviews, 79, 111–121, 2013.

Dyke, A.S. and Savelle, J.M.: Holocene history of the Bering Sea bowhead whale (*Balaena mysticetus*) in Its Beaufort Sea summer grounds off southwestern Victoria Island, western Canadian Arctic, Quaternary Research, 55, 371–379, 2001.

Elias, S., Short, S.K., and Phillips, R.L.: Paleoecology of late-glacial peats from the Bering land bridge, Chukchi Sea shelf region, northwestern Alaska, Quaternary Research, 38, 371–378, 1992.

Elvelhøi, A. and Rønningsland, T.M.: Semiquantitative calculation of the relative amounts of kaolinite and chlorite by X-ray diffraction, Marine Geology, 27, M19-M23, 1978.

Farmer, J.R., Cronin, T.M., de Vernal, A., Dwyer, G.S., Keigwin, L.D., and Thunell, R.C.: Western Arctic Ocean temperature variability during the last 8000 years, Geophysical Research Letters, 38, L24602, 2011.

Funder, S. et al.: A 10,000-year record of Arctic Ocean sea-ice variability–View from the beach, Science, 333, 747–750, 2011.

Giles, K.A. et al.: Western Arctic Ocean freshwater storage increased by wind-driven spin-up of the Beaufort Gyre, Nature Geoscience, 5, 194–197, 2012.

Clim. Past Discuss., doi:10.5194/cp-2016-105, 2016
Manuscript under review for journal Clim. Past
Published: 31 October 2016

Godfrey, J.S.: A sverdrup model of the depth-integrated flow for the ocean allowing for island circulations, Geophysical and Astrophysical Fluid Dynamics, 45, 89–112, 1989.

Griffin, G.M. and Goldberg, E.D.: Clay mineral distributions in the Pacific Ocean. In Hill, M.N. (ed) The sea, III, p. 728-741, New York, Interscience Pub., 1963.

Gudkovitch, Z.M.: On the nature of the Pacific current in Bering Strait and the cause of its seasonal variations, Deep-Sea Research, 9, 507–510, 1962.

Harada, N.: Review: Potential catastrophic reduction of sea ice in the western Arctic Ocean: its impact on biogeochemical cycles and marine ecosystems, Global and Planetary Change, 136, 1–17, 2016.

Hasumi, H.: Sensitivity of the global thermohaline circulation to interbasin freshwater transport by the atmosphere and the Bering Strait throughflow, Journal of Climate, 15, 2516–2526, 2002.

Hetzinger, S., Halfar, J., Mecking, J.V., Keenlyside, N.S., Kronz, A., Steneck, R.S., Adey, W.H., and Lebednik, P.A.: Marine proxy evidence linking decadal North Pacific and Atlantic climate, Climate Dynamics, 39, 1447–1455, 2012.

Heusser, C.J., Heusser, L.E., and Peteet, D.M.: Late-Quaternary climate change on the American North Pacific coast, Nature 315, 485–487, 1985.

Honda, M., Nakamura, H., Ukita, J., Kousaka, I., and Takeuchi, K.: Interannual seesaw between Aleutian and Icelandic lows. Part I: Seasonal dependence and life cycle, Journal of Climate, 14, 1029–1042, 2001.

Hu, A., Meehl, G.A., Han, W., Otto-Bliestner, B., Abe-Ouchi, A., and Rosenbloom, N.: Effects of the Bering Strait closure on AMOC and global climate under different background climates, Progress in Oceanography, 132, 174–196, 2015.

Clim. Past Discuss., doi:10.5194/cp-2016-105, 2016
Manuscript under review for journal Clim. Past
Published: 31 October 2016

Kaufman, D.S. et al.: Holocene climate changes in eastern Beringia (NW North America) – a systematic review of multi-proxy evidence, Quaternary Science Reviews, 147, 312–339, 2016.

Kalinenko, V.V.: Clay minerals in sediments of the Arctic Seas. Lith. Min. Res. 36, 362–372. Translated from Litologiya I Poleznye Iskopaemye 4, 418–429, 2001.

Katsuki, K., Khim, B.-K., Itaki, T., Harada, N., Sakai, H., Ikeda, T., Takahashi, K., Okazaki, Y., and Asahi, H.: Land–sea linkage of Holocene paleoclimate on the Southern Bering Continental Shelf, The Holocene, 19, 747–756, 2009.

Keigwin, L.D., Donelly, J.P., Cook, M.S., Driscoll, N.W., and Brigham-Grette, J.: Rapid sea-level rise and Holocene climate in the Chukchi Sea, Geology, 34, 861–864, 2006.

Keigwin, L.D. and Cook, M.S.: A role for North Pacific salinity in stabilizing North Atlantic climate, Paleoceanography, 22, PA3102, 2007.

Kobayashi, D., Yamamoto, M., Irino, T., Nam, S.-I., Park, Y.-H., Harada, N., Nagashima, K., Chikita, K., and Saitoh, S.-I.: Distribution of detrital minerals and sediment color in western Arctic Ocean and northern Bering Sea sediments: Changes in the provenance of western Arctic Ocean sediments since the last glacial period, Polar Science, in press

Leduc, G., Vidal, L., Tachikawa, K., Rostek, F., Sonzogni, C., Beaufort, L. and Bard, E.: Moisture transport across Central America as a positive feedback on abrupt climatic changes, Nature, 445, 908–911, doi:10.1038/nature05578, 2007.

McKay, J. L. et al.: Holocene fluctuations in Arctic sea-ice cover: dinocyst-based reconstructions for the eastern Chukchi Sea, Canadian Journal of Earth Sciences, 45, 1377–1397, 2008.

Clim. Past Discuss., doi:10.5194/cp-2016-105, 2016
Manuscript under review for journal Clim. Past
Published: 31 October 2016

McManus, J.F., Francois, R., Gherardi, J.-M., Keigwin, L.D., and Brown-Leger, S.: Collapse and rapid resumption of Atlantic meridional circulation linked to deglacial climate changes, Nature, 428, 834–837, 2004.

McNeely, R., Dyke, A.S., and Southon, J.R.: Canadian marine reservoir ages, preliminary data assessment, Open File Report-Geological Survey of Canada, 5049, no. 3, 2006.

Naidu, A.S., Creager, J.S., and Mowatt, T.C.: Clay mineral dispersal patterns in the North Bering and Chukchi Seas, Marine Geology, 47, 1-15, 1982.

Naidu, A.S. and Mowatt, T.C.: Sources and dispersal patterns of clay minerals in surface sediments from the continental shelf areas off Alaska, Geological Society of America Bulletin, 94, 841–854, 1983.

Nwaodua, E., Ortiz, J.D., and Griffith, E.M.: Diffuse spectral reflectance of surficial sediments indicates sedimentary environments on the shelves of the Bering Sea and western Arctic, Marine Geology, 355, 218–233, 2014.

Olsen, J., Anderson, N.J., and Knudsen, M.F.: Variability of the North Atlantic Oscillation over the past 5,200 years, Nature Geoscience, 5, 808–812, 2012.

Oppo, D.W., McManus, J.F., and Cullen, J.L.: Deepwater variability in the Holocene epoch, Nature, 422, 277–278, 2003.

Ortiz, J.D., Polyak, L., Grebmeier, J.M., Darby, D., Eberl, D.D., Naidu, S., and Nof, D.: Provenance of Holocene sediment on the Chukchi-Alaskan margin based on combined diffuse spectral reflectance and quantitative X-Ray Diffraction analysis, Global Planetary Change, 68, 73–84, 2009.

Ortiz, J.D., Nof, D., Polyak, L., St-Onge, G., Lisé-Pronovost, A., Naidu, S., Darby, D., and Brachfeld, S.: The late Quaternary flow through the Bering Strait has been forced by the Southern Ocean winds. Journal of Physical Oceanography, 42, 2014–2029, 2012.

Osterberg, E.C., Mayewski, P.A., Fisher, D.A., Kreutz, K.J., Maasch, K.A., Sneed, S.B., and Kelsey, E.: Mount Logan ice core record of tropical and solar influences on Aleutian Low variability: 500–1998 A.D. Journal of Geophysical Research, Atmosphere, 119, 11,189–11,204, doi:10.1002/2014JD021847, 2014.

Overland, J.O., Adams, J. M., and Bond, N.: Decadal variability of the Aleutian Low and its relation to high-latitude circulation, Journal of Climate, 12, 1542–1548, 1999.

Paillard, D., Labeyrie, L., and Yion, P.: Macintosh program performs time-series analysis, EOS Trans. AGU 77, 379, 1996.

Petschick, R.: MacDiff 4.2.6. [online] available at http://www.geol-pal.uni-frankfurt.de/Staff/Homepages/Petschick/MacDiff/MacDiff%20Latest%20infoE.html, 2000.

Pickart, R.S.: Shelfbreak circulation in the Alaskan Beaufort Sea: Mean structure and variability, Journal of Geophysical Research 109, C04024, 2004.

Pickart, R.S., Pratt, L.J., Torres, D.J., Whitledge, T.E., Proshutinsky, A.Y., Aagaard, K., Agnewd, T.A., Moore, G.W.K., and Dail, H.J.: Evolution and dynamics of the flow through Herald Canyon in the western Chukchi Sea, Deep-Sea Research II, 57, 5–26, 2010.

Polyak, L., Belt, S., Cabedo-Sanz, P., Yamamoto, M., and Park, Y.-H.: Holocene sea-ice conditions and circulation at the Chukchi-Alaskan margin, Arctic Ocean, inferred from biomarker proxies, The Holocene, in press.

Clim. Past Discuss., doi:10.5194/cp-2016-105, 2016
Manuscript under review for journal Clim. Past
Published: 31 October 2016

Porter, S.E.: Assessing whether climate variability in the Pacific Basin influences the climate over the North Atlantic and Greenland and modulates sea ice extent, Ph.D. Thesis, Ohio State University, 222 p, 2013.

Proshutinsky, A.Y. and Johnson, M.A.: Two circulation regimes of the wind-driven Arctic Ocean, Journal of Geophysical Research, 102 (C6), 12493–12514, 1997.

Reimer, P.J., et al.: Intcal13 and Marine13 radiocarbon age calibration curves 0–50,000 years cal BP., Radiocarbon, 55, 1869–1887, 2013.

Richter, I. and Xie, S.: Moisture transport from the Atlantic to the Pacific basin and its response to North Atlantic cooling and global warming, Climate Dynamics, 35, 551–566, doi:10.1007/s00382-009-0708-3, 2010.

Rigor, I. G. et al.: Response of sea ice to the Arctic Oscillation, Journal of Climate, 15, 2648–2663, 2002.

Rimbu, N., Lohmann, G., Kim, J.-H., Arz, H.W., and Schneider, R.: Arctic/North Atlantic Oscillation signature in Holocene sea surface temperature trends as obtained from alkenone data, Geophysical Research Letters, 30, 1280. doi:10.1029/2002GL016570, 2003.

Roach, A.T., Aagaard, K., Pease, C.H., Salo, S.A., Weingartner, T., Pavlov, V., and Kulakov, M.: Direct measurements of transport and water properties through Bering Strait, Journal of Geophysical Research, 100, 18433–18457, 1995.

Sandal, C. and Nof, D.: The Collapse of the Bering Strait Ice Dam and the Abrupt Temperature Rise in the Beginning of the Holocene, Journal of Physical Oceanography, 38, 1979–1991, 2008.

Sarnthein, M., Gebhardt, H., Kiefer, T., Kucera, M. Cook, M., and Erlenkeuserd, H.: Mid Holocene origin of the sea-surface salinity low in the subarctic North Pacific, Quaternary Science Reviews, 23, 2089–2099, 2004.

Screen, J.A. and Simmonds, I.: The central role of diminishing sea ice in recent Arctic temperature amplification, Nature, 464, 1334–1337, 2010.

Serreze M.C., Maslanik J.A., Key J.R., and Kokaly R.F.: Diagnosis of the record minimum in Arctic sea ice area during 1990 and associated snow cover extremes, Geophysical Research Letters, 22, 2183–2186, 1995.

Shaffer, G. and Bendtsen, J.: Role of the Bering Strait in controlling North Atlantic ocean circulation and climate, Nature, 367, 354–357, 1994.

Shimada, K., Carmack, E., Hatakeyama, K., and Takizawa, T.: Varieties of shallow temperature maximum waters in the Western Canadian Basin of the Arctic Ocean, Geophysical Research Letters, 28, 3441–3444, 2001.

Shimada, K., Kamoshida, T., Itoh, M., Nishino, S., Carmack, E., McLaughlin, F., Zimmermann, S., and Proshutinsky, A.: Pacific Ocean inflow: Influence on catastrophic reduction of sea ice cover in the Arctic Ocean, Geophysical Research Letters, 33, L08605, 2006.

Shtokman, V.B.: Vliyanie vetra na techeniya v Beringovo Prolive, prichiny ikh bol'shikh skorostei i preobladayueshego severnogo napravleniya, Trans. Inst. Okeanolog., Akad. Nauk SSSR, 25, 171– 197, 1957.

Singh, H.K.A., Donohoe, A., Bitz, C.M., Nusbaumer, J., and Noone, D.C.: Greater aerial moisture transport distances with warming amplify interbasin salinity contrasts. Geophysical Research Letters 43, 8677–8684, doi:10.1002/2016GL069796, 2016.

Clim. Past Discuss., doi:10.5194/cp-2016-105, 2016
Manuscript under review for journal Clim. Past
Published: 31 October 2016

Solignac, S., Seidenkrantz, M.-S., Jessen, C., Kuijpers, A., Gumvald, A.K., and Olsen, J.: Late-Holocene sea-surface conditions offshore Newfoundland based on dinoflagellate cysts, Holocene, 21, 539–552, 2011.

Stein R.: Developments in Marine Geology: Arctic Ocean Sediments: Processes, Proxies, and Paleoenvironment, Elsevier, Amsterdam, 529p, 2008.

Steinman, B.A., Abbott, M.B., Mann, M.E., Ortiz, J.D., Feng, S., Pompeani, D.P., Stansell, N.D., Anderson, L., Finney, B.P., and Bird, B.W.: Ocean-atmosphere forcing of centennial hydroclimate variability in the Pacific Northwest, Geophysical Research Letters, 41, doi:10.1002/2014GL059499, 2014.

Steinhilber, F., Beer, J., and Fröhlich, C.: Total solar irradiance during the Holocene, Geophysical Research Letters, 36, L19704, doi:10.1029/2009GL040142, 2009.

Stigebrandt, A.: The North Pacific: A global-scale estuary, Journal of Physical Oceanography, 14, 464–470, 1984.

Sun, J. and Tan, B.: Mechanism of the wintertime Aleutian Low–Icelandic Low seesaw, Geophysical Research Letters, 40, 4103–4108, 2013.

Thornalley, D.J.R., Elderfield, H., and McCave, I.N.: Holocene oscillations in temperature and salinity of the surface subpolar North Atlantic, Nature, 457, 711–714, 2009.

Thompson, D.W.J. and Wallace, J.M.: The Arctic Oscillation signature in the wintertime geopotential height and temperature fields, Geophysical Research Letters, 25, 1297–1300, 1998.

Vare L.L., Masse G., and Gregory, T.R.: Sea ice variations in the central Canadian Arctic Archipelago during the Holocene, Quaternary Science Reviews, 28, 1354–1366, 2009.

Vogt, C.: Regional and temporal variations of mineral assemblages in Arctic Ocean sediments as climatic indicator during glacial/interglacial changes, Reports on Polar Research, 251, 1–309, 1997.

Weingartner, T., Aagaard, K., Woodgate, R., Danielson, S., Sasaki, Y., and Cavalieri, D.: Circulation on the north central Chukchi Sea shelf, Deep-Sea Research II, 52, 3150–3174, 2005.

Winsor, P. and Chapman, D.C.: Pathways of Pacific water across the Chukchi Sea: A numerical model study, Journal of Geophysical Research, 109, C03002, doi:10.1029/2003JC001962, 2004.

Woodgate, R.A. and Aagaard, K., 2005: Revisiting the Bering Strait freshwater flux into the Arctic Ocean, Geophysical Research Letters, 32, L02602, 2005.

Clim. Past Discuss., doi:10.5194/cp-2016-105, 2016
Manuscript under review for journal Clim. Past
Published: 31 October 2016

Climate of the Past Discussions
Open Access

Table 1. Radiocarbon ages of moluscan shells in core ARA-02B 01A-GC

			ΔR = 0		ΔR = 500		
Depth	Conventional age	±	Calendar age	±	Calendar age	±	UGAMS
cm	years	years	years BP	years	years BP	years	number
107.5	3740	30	3709	51	3057	58	11825
159.5	4370	30	4497	54	3842	52	11826
204.5	4860	30	5187	70	4482	50	11827
241.5	5180	30	5544	39	4893	46	11828
347.5	6110	30	6539	51	5991	56	11829
456.5	7690	30	8149	50	7644	36	11830
509.5	8670	30	9350	47	8642	56	11831

Figure captions

Fig. 1. Index map showing location of cores ARA02B 01A-GC (this study), HLY0501-05JPC/TC (this study and Farmer et al., 2011), HLY0501-06JPC (Ortiz et al., 2009), and HLY0205-GGC19 (Farmer et al., 2011), as well as surface sediment samples (Kobayashi et al., 2016, with additions). BSI = Bering Strait inflow, BC = Barrow Canyon, HN = Hanna Shoal, and HR = Herald Shoal. BG = Beaufort Gyre, ACC = Alaskan Coastal Current, SBC = Subsurface Boundary Current, ESCC = East Siberian Coastal Current, TPD = Transpolar Drift. Red, yellow and blue arrows indicate BSI branches. AO+ and AO– indicate circulation in the positive and negative phases of the Arctic Oscillation, respectively.

Fig. 2. Spatial distributions of the diffraction intensity ratios of (A) feldspar to quartz (Q/F), and of (B) chlorite+kaolinite and (C) chlorite to illite (KC/I and C/I, respectively) of bulk sediments, and (D) the longitudinal distribution of the Q/F ratio in the western Arctic (>65°N) and (E) the latitudinal distribution of the KC/I and C/I ratios in the Bering Sea and the western Arctic (>150°W). Data from Kobayashi et al. (2016) with additions for the Beaufort Sea.

Fig. 3. Changes in (A) quartz/feldspar (Q/F) ratio of bulk sediment, (B) (chlorite + kaolinite)/illite (KC/I) and chlorite/illite (C/I) ratios with 1σ-intervals (analytical error) of clay fraction (Supplementary Table 2), and (C) linear sedimentation rates (LSR) in core ARA02B 01A-GC during the last ca. 9.3 ka.

Fig. 4. Changes in (A) quartz/feldspar (Q/F) ratio, (B) (chlorite + kaolinite)/illite (KC/I) and chlorite/illite (C/I) ratios of bulk sediment, and (C) linear sedimentation rates (LSR) in core HLY0501-05JPC/TC, and (D) index of chlorite abundance based on Diffuse Spectral Reflectance in core HLY0501-06JPC (Ortiz et al., 2009) during the last ca. 9.3 ka.

Fig. 5. Changes in (A) quartz/feldspar (Q/F) ratio in core ARA02B 01A-GC (black line: 5-point moving average) and HLY0501-05JPC/TC, and the June insolation at 75°N during the Holocene, and (B) detrended variations in the quartz/feldspar (Q/F) ratio in logarithmic scale in core ARA02B 01A-GC and the solar irradiance (TSI) during the Holocene (Steinhilber et al., 2009), with 400-year moving averages and 1,000-year filtered variations indicated by colored and black lines, respectively. The detrended values were obtained by cubic polynomial regression.

Fig. 6. Schematic map showing the distribution of summer sea ice and the rotation of the Beaufort Gyre (BG) in the early, middle and late Holocene, inferred from the quartz/feldspar (Q/F) proxy record. Also shown is the Bering Strait inflow (BSI) intensity inferred from the (chlorite + kaolinite)/illite (KC/I) and chlorite/illite (C/I) ratios. Red arrow indicates the drift path of Kara Sea grains (KSG; Darby et al., 2012).

Fig. 7. Max Entropy power spectra of variation in the quartz/feldspar ratio in core ARA02B 01A-GC (N = 110, m = 47) and the total solar irradiance (N = 932, m = 140) (Steinhilber et al., 2009) during the last 9.3 ka.

Fig. 8. Changes in (A) (chlorite + kaolinite)/illite (CK/I) and chlorite/illite (C/I) ratios in core ARA02B 01A-GC, (B) IP_{25} concentrations in HLY0510-5JPC (Polyak et al., 2016), and (C) sea ice cover concentration estimated from dinoflagellate cyst assemblages in cores 05JPC and GGC19 (Farmer et al., 2011).

Fig. 9. Changes in (A) (chlorite + kaolinite)/illite (CK/I) and chlorite/illite (C/I) ratios in core ARA02B 01A-GC, (B) *Neogloboquadrina pachyderma* (dextral) Mg/Ca-derived near-surface temperature with the 5-point running mean in ODP Site 984 (Came et al., 2007), (C) *Globorotalia inflata* $\delta^{18}O$ and Mg/Ca-derived subthermocline salinity in core RAPiD-12-1K (Thornalley et al., 2009), (D) *Islandinium minutum* abundance in cores 03G and 12G (Solignac et al., 2011), (E) benthic foraminifera $\delta^{13}C$ in ODP Site 980 (Oppo et al., 2003), and Pa/Th ratio in core OCE326-GGC5 (McManus et al., 2004) from the North Atlantic. Blue shades in panels A and B–D indicate periods of stronger BSI and the North Atlantic SPG circulation, respectively.

Fig. 10. Inferred atmospheric conditions and ocean circulation in the northern high latitudes in the middle and late Holocene. Also shown are locations of ODP Site 984 (Came et al., 2007), core RAPiD-12-1K (Thornalley et al., 2009), and cores AI07-3G and AI07-12G (Solignac et al., 2012). BSI = Bering Strait Inflow, NAD = North Atlantic Drift, IC = Irminger Current, LC = Labrador Current, DWF = center of deep-water formation, IL = Icelandic Low, AL = Aleutian Low. Red and blue arrows indicate the flows of saline and less saline waters, respectively.

Climate of the Past
Discussions
Open Access

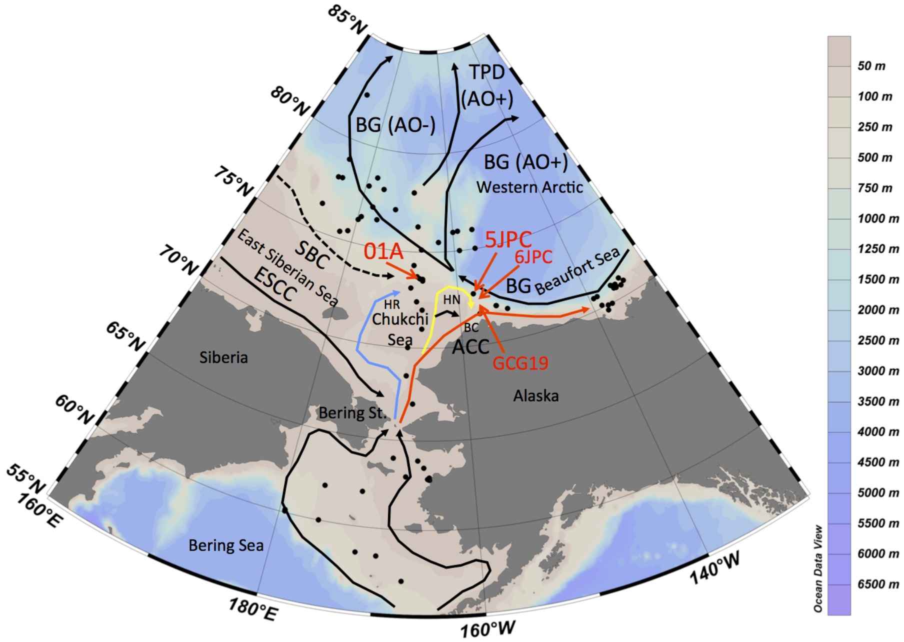

Fig. 1

Clim. Past Discuss., doi:10.5194/cp-2016-105, 2016
Manuscript under review for journal Clim. Past
Published: 31 October 2016

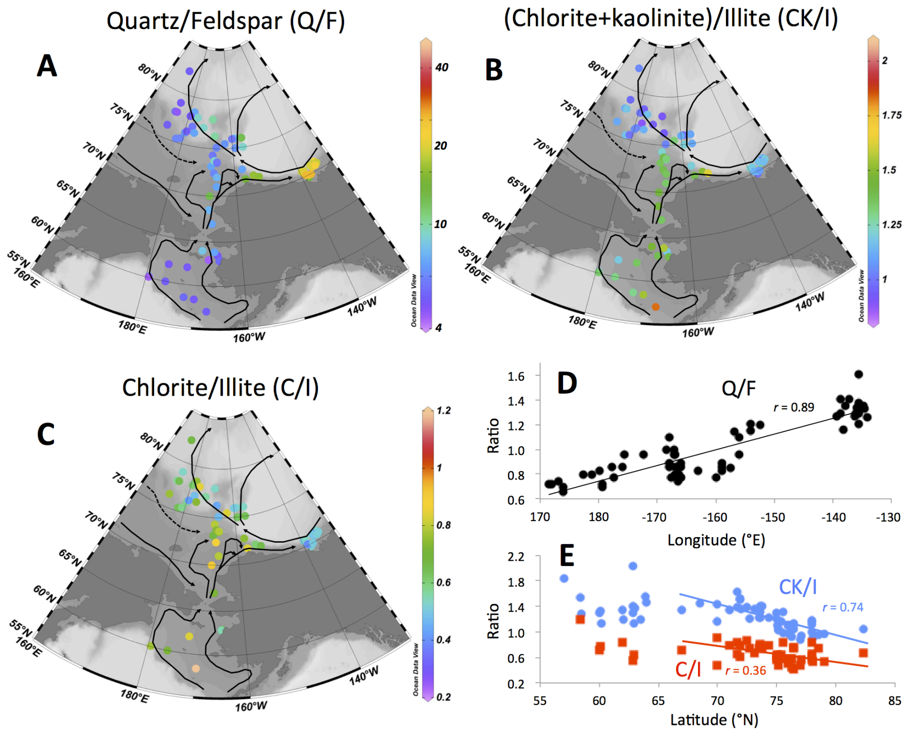

925

926 Fig. 2

927

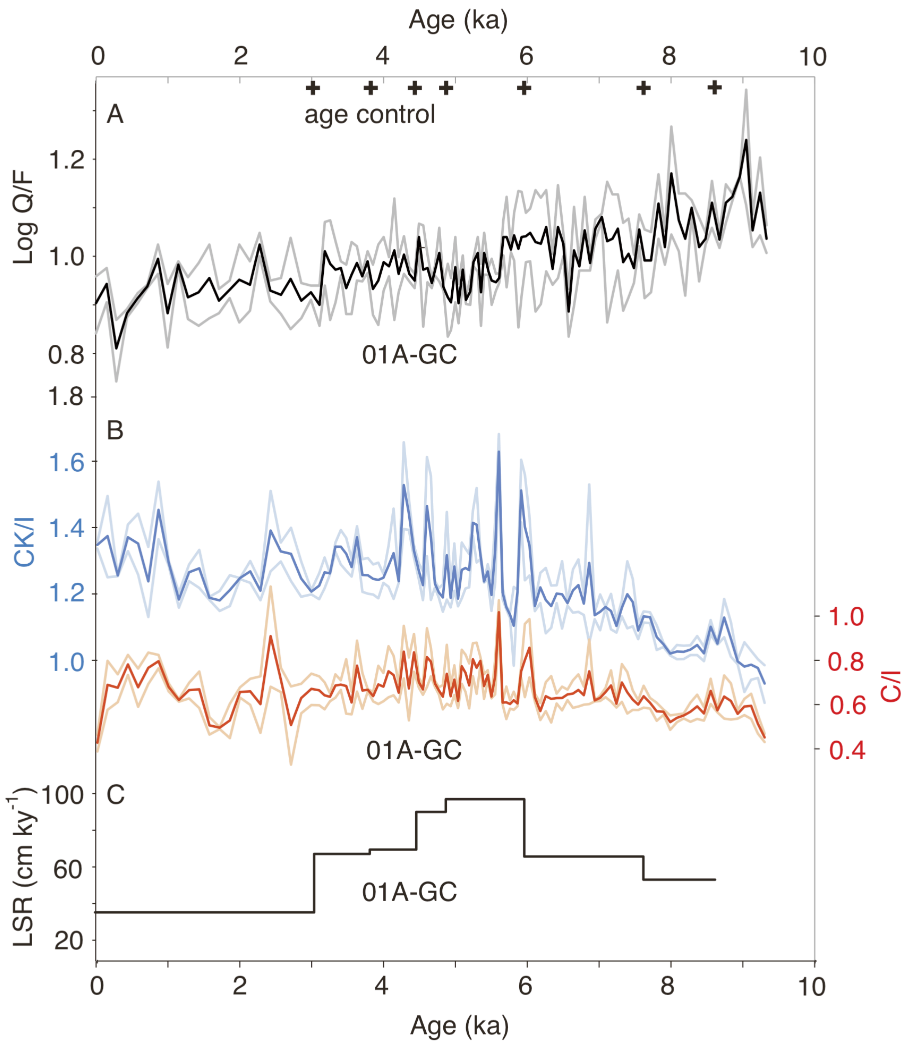
Age (ka)
0
2
4
6
8
10
A
age control
Log Q/F
1.2
1.0
0.8
01A-GC
1.8
B
1.6
1.4
CK/I
1.2
1.0
1.0
0.8
0.6
0.4
C/I
01A-GC
100
C
LSR (cm ky-1)
60
20
01A-GC
Age (ka)

Fig. 3

Clim. Past Discuss., doi:10.5194/cp-2016-105, 2016
Manuscript under review for journal Clim. Past
Published: 31 October 2016

Climate of the Past Discussions

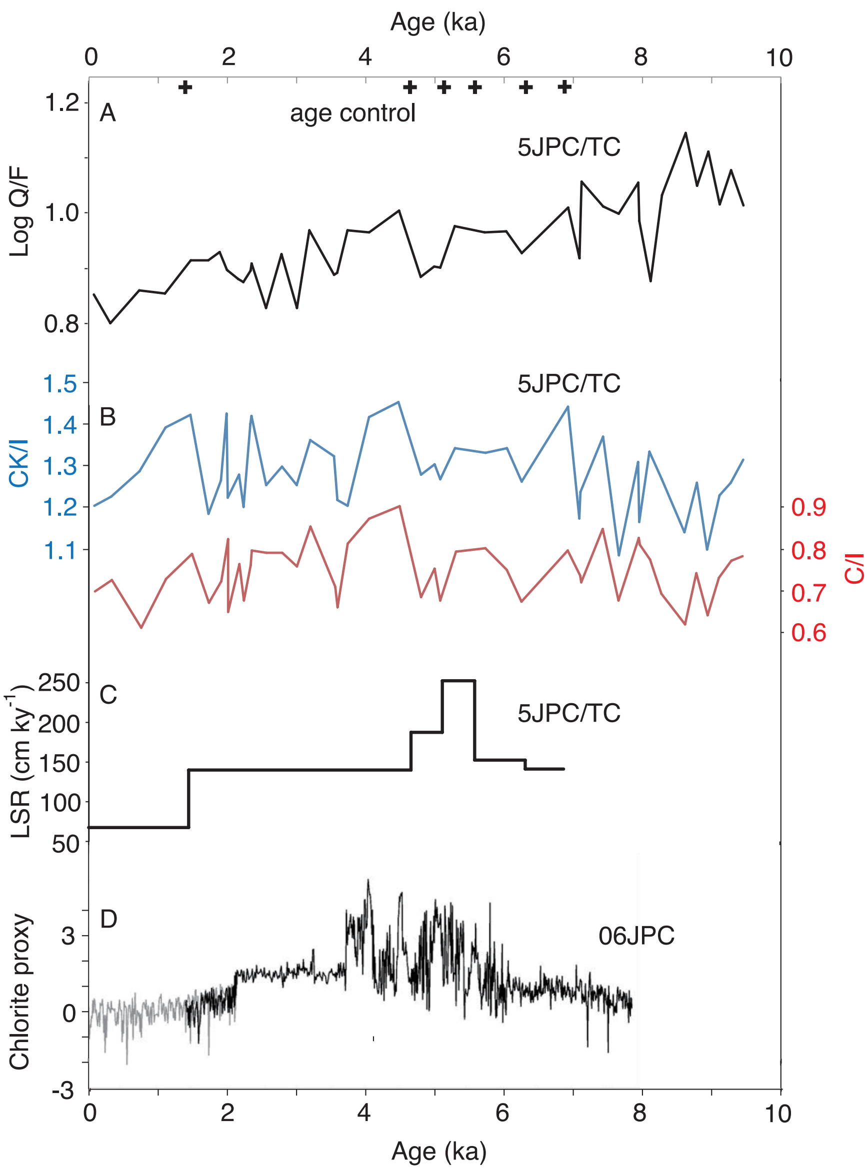

931
932 Fig. 4
933

Clim. Past Discuss., doi:10.5194/cp-2016-105, 2016
Manuscript under review for journal Clim. Past
Published: 31 October 2016

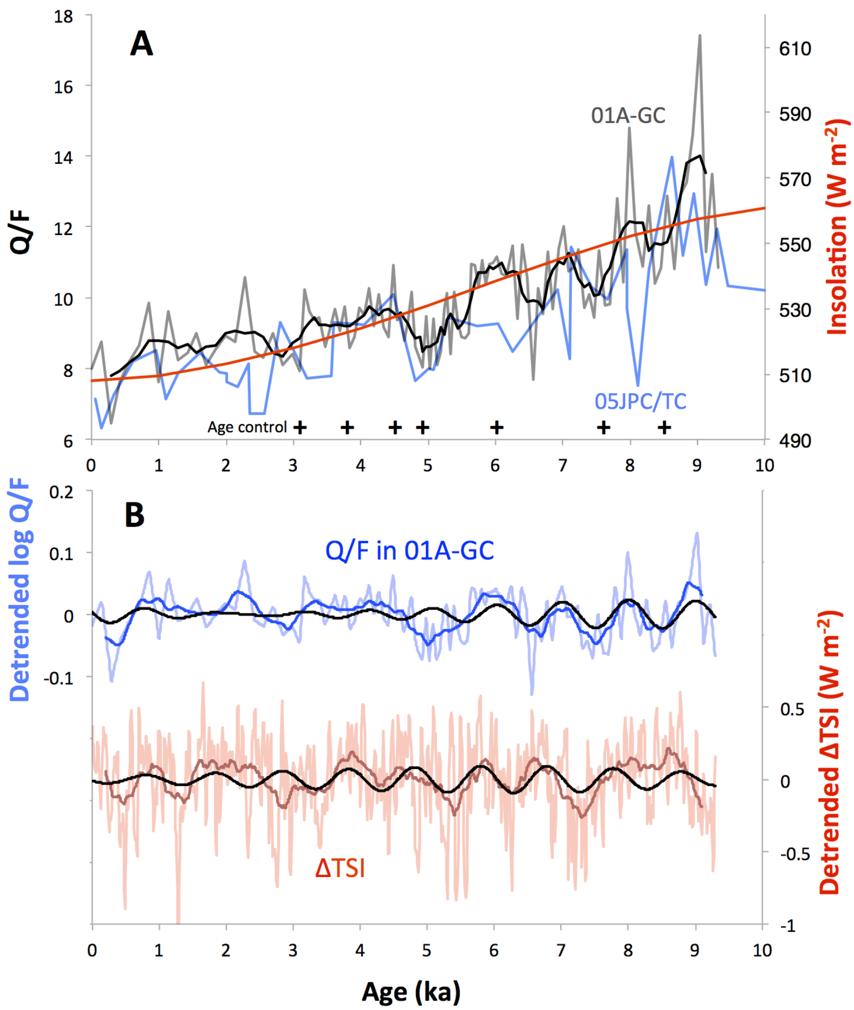

Fig. 5

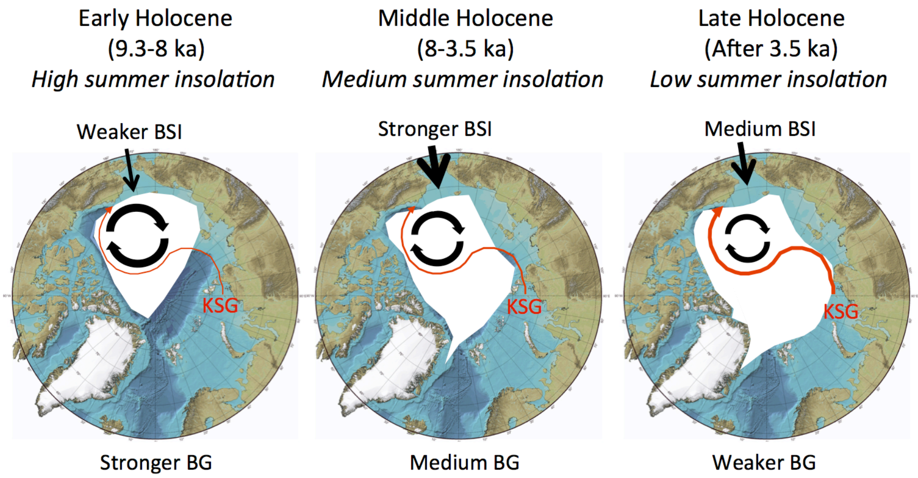
Early Holocene
(9.3-8 ka)
High summer insolation
Middle Holocene
(8-3.5 ka)
Medium summer insolation
Late Holocene
(After 3.5 ka)
Low summer insolation
Weaker BSI
Stronger BSI
Medium BSI
KSG
KSG
KSG
Stronger BG
Medium BG
Weaker BG

Fig. 6

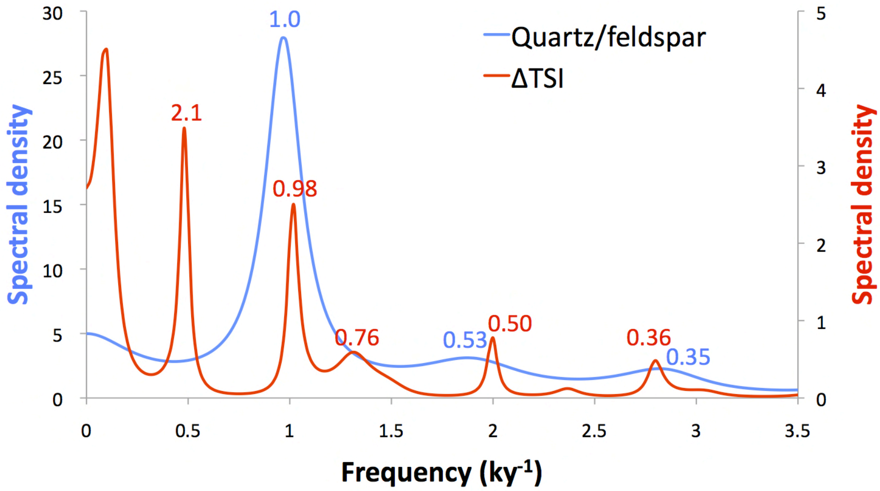

940
941 Fig. 7
942

Clim. Past Discuss., doi:10.5194/cp-2016-105, 2016
Manuscript under review for journal Clim. Past
Published: 31 October 2016

Climate of the Past Discussions

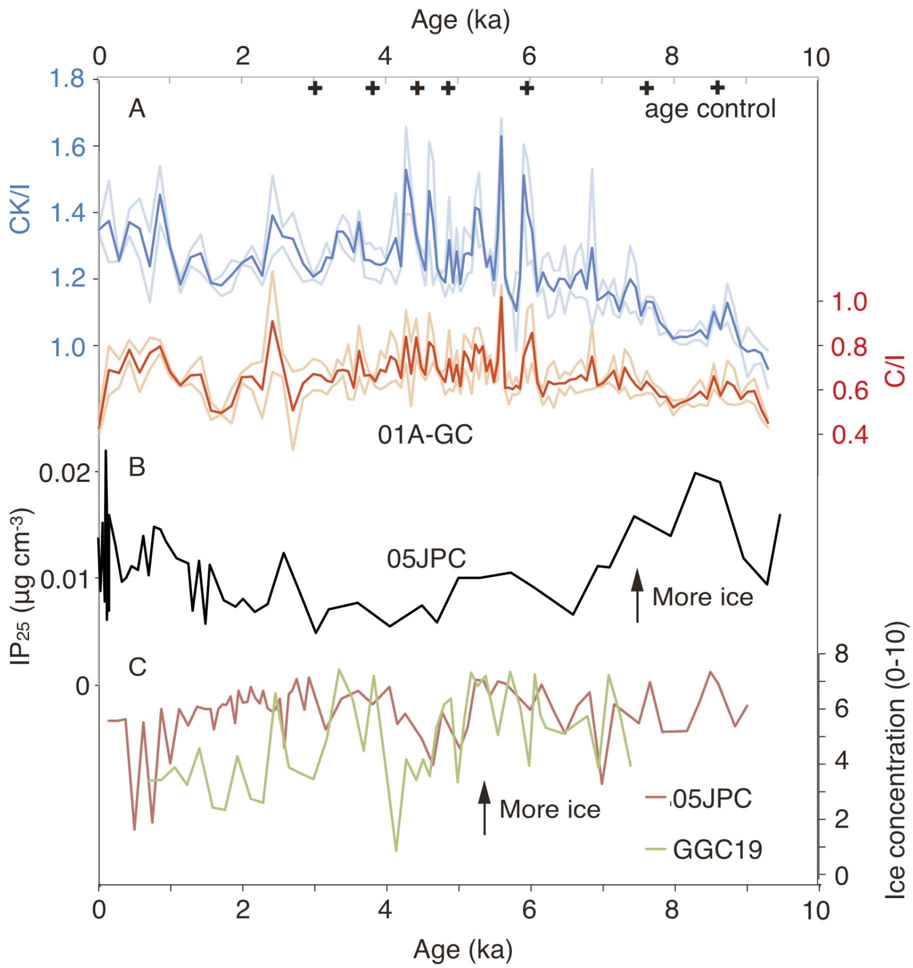

943

944 Fig. 8

945

Clim. Past Discuss., doi:10.5194/cp-2016-105, 2016
Manuscript under review for journal Clim. Past
Published: 31 October 2016

Climate of the Past Discussions

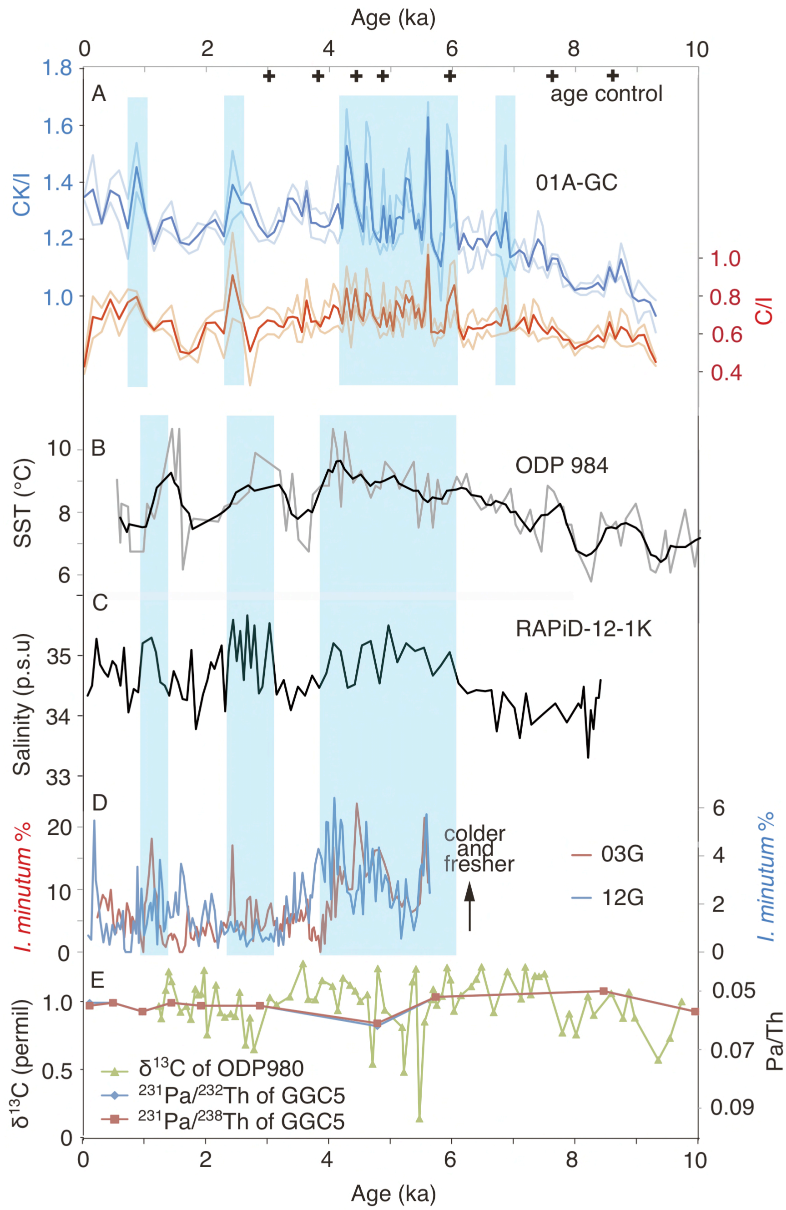

946

947 Fig.9

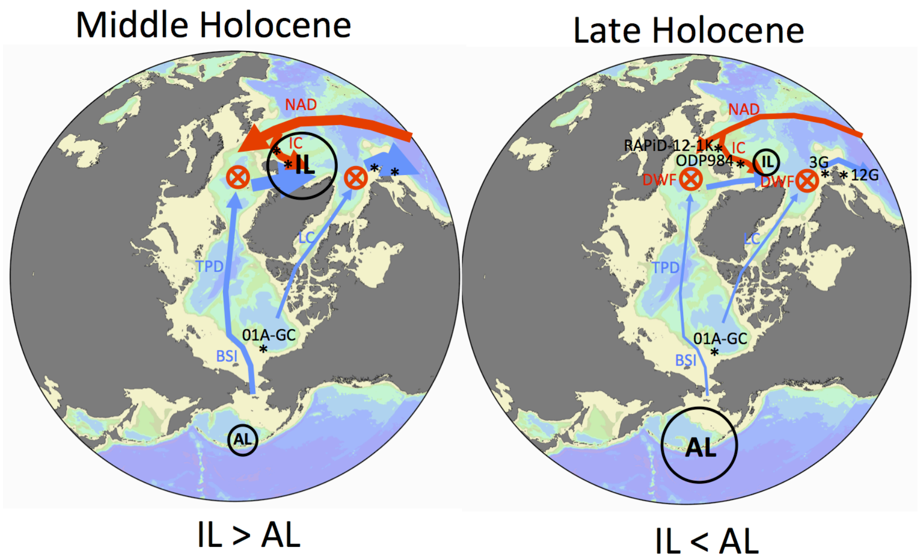
Middle Holocene
NAD
IC
IL
LC
TPD
01A-GC
BSI
AL
IL > AL
Late Holocene
NAD
RAPiD-12-1K
IC
ODP984
IL
DWF
DWF
3G
12G
LC
TPD
01A-GC
BSI
AL
IL < AL

Fig. 10